β-Catenin in the Fibroproliferative Response to Acute Lung Injury

Ivor S. Douglas, Fernando Diaz del Valle, Robert A. Winn, and Norbert F. Voelkel

Department of Medicine, Pulmonary Sciences and Critical Care Medicine, University of Colorado Health Sciences Center; and Denver Health Medical Center, Denver, Colorado

Resolution of alveolar epithelial/capillary membrane damage after acute lung injury requires coordinated and effective tissue repair to reestablish a functional alveolar epithelial/capillary membrane barrier. We hypothesized that signaling pathways important in lung alveolar bud ontogeny are activated in the recovery and remodeling phases after profound oxidant stress lung injury in a murine model. To test this, we characterized the expression of noncanonical β-catenin pathway proteins E-cadherin, integrin-linked kinase–1, and β-catenin in mice undergoing normoxic recovery after exposure to butylated hydroxytoluene (BHT, ionol) and concomitant sublethal (75% O_2) hyperoxia. Mice developed early acute lung injury with subsequent inflammation, collagen deposition, interstitial cellular proliferation, and lung architectural distortion. Reduced E-cadherin expression after 6 d of BHT and hyperoxia was accompanied by enhanced expression and nuclear localization of β-catenin and increased integrin-linked kinase-1 expression during subsequent normoxic recovery. This resulted in increased expression of the cotranscriptional regulators TCF-1 and -3 and cyclin D1. Proliferation of murine lung epithelial-12 cells *in vitro* after 8 h of treatment with BHT quinone-methide and hyperoxia and 48 h of normoxic recovery was enhanced 2.7-fold compared with vehicle-treated control mice at the same time point. BHT/hyperoxia-exposed mice treated with the pan-caspase inhibitor z-ASP had increased acute lung injury and reduced survival despite the presence of TUNEL-positive cells, suggesting enhanced lung cell necrosis. β-Catenin expression was reduced in z-ASP–co-treated lungs after BHT/hyperoxia. The noncanonical cadherin–β-catenin axis is associated with fibroproliferative repair after BHT/hyperoxia exposure and may regulate epithelial proliferation and lung matrix remodeling and repair in response to lung injury.

Keywords: β-catenin; E-cadherin; lung injury repair; cell junctions; caspase

Resolution of alveolar epithelial/capillary membrane damage after acute lung injury (ALI) requires coordinated and effective tissue reconstruction to reestablish a functional barrier. In particular, restoration of the normal air space architecture requires reconstitution of denuded type I alveolar epithelial cells that undergo apoptotic and necrotic death during the exudative phase of ALI. Coordination of extracellular matrix turnover and regeneration of type II epithelial cells is important in reestablishing surfactant production and ion transport (1). Orderly re-epithelialization suppresses fibroblast proliferation and matrix deposition after ALI (1, 2). However, resolution of ALI can result in disordered repair of the alveolus, characterized by impaired fibrinolysis of the inflammatory coagulum, fibrocellular proliferation, architectural distortion of the lung parenchyma, and impaired angiogenesis. Clinically, the result of this fibroproliferative phase of ALI in survivors is a restrictive ventilatory defect and evidence of impaired alveolar membrane function characterized by a prolonged reduction in the diffusing capacity for carbon monoxide (3).

The cellular regulatory mechanisms necessary for coordinating functional repopulation and reconstitution of the alveolar/capillary membrane remain unclear. Transdifferentiation of epithelial cells into matrix producing fibroblasts and myofibroblasts with enhanced matrix turnover has been suggested as one mechanism by which disordered epithelial remodeling promotes progression to the fibroproliferation in idiopathic pulmonary fibrosis (IPF) (4) and ALI (5). Several lines of investigation suggest that the mechanisms of resolution and lung injury repair in adults are controlled in part by regulatory pathways that are important in lung morphogenesis and development (4, 6). Deregulation of these pathways may result in amplification of the initial injury and disorderly repair, with fibrosis or neoplastic degeneration (6).

The Wnt pathway has been identified as one of the numerous signaling pathways critical for precise temporal and spatial control of lung morphogenesis (7, 8). The centrality of β-catenin as a key regulatory protein in the Wnt cascade is conferred by its bidirectional capacity to tightly regulate nuclear transcription and to affect cell migration and adhesion by closely interacting with the cytoskeleton and adherens junction cadherins. Conditional targeted deletion of β-catenin from the alveolar epithelium of developing mouse embryos results in complete disruption of peripheral terminal alveolar saccule formation and disturbances of pulmonary vasculogenesis (9, 10). β-Catenin expression is induced in type II epithelial cells from hyperoxia-exposed rats (11). In humans, β-catenin activation has been implicated in several chronic pulmonary disorders, including IPF. Chilosi and coworkers (6) have documented nuclear localization of β-catenin in type II epithelial cells and fibroblastic focus spindle cells in IPF lungs, which is consistent with activation of the β-catenin pathway in these proliferative lesions.

We hypothesized that β-catenin signaling is upregulated in the reparative remodeling response to acute lung injury. We studied the lungs of mice in the normoxic recovery phase after a well characterized, profound, oxidant-mediated injury induced by butylated hydroxytoluene (BHT, ionol) and concomitant sublethal (75% O_2) hyperoxic exposure. BHT and its metabolite, BHT quinone-methide (BHT-QM), inhibit antioxidants (12) and interact with oxygen in aqueous media to release reactive oxygen species, including $O_2\cdot$ anion (13). Additional pneumotoxic effects of BHT have been reported (14). The proliferative repair response in the BHT/O_2 ALI model, initially described by Witschi and Haschek (15–17), is characterized by initial monocyte-predominant acute pulmonary inflammation and type I epithelial cell necrosis. Upon return to a normoxic environment, compensatory type II epithelial and interstitial cell proliferation occurs (16–20). Long-lasting morphologic changes, reminiscent of late-phase ALI, persist out to 1 yr after the initial insult. This proliferative phase is also characterized by collagen deposition and a

(*Received in original form July 20, 2005 and in final form September 26, 2005*)

This work was supported in part by NIH-K08HL070940.

Correspondence and requests for reprints should be addressed to Ivor S. Douglas, M.D., Univ. of Colorado at Denver & Health Sciences Center, Pulmonary Sciences & Critical Care Medicine SOM 5226, C-272, Denver, CO 80262. E-mail: idouglas@dhha.org

Am J Respir Cell Mol Biol Vol 34. pp 274–285, 2006
Originally Published in Press as DOI: 10.1165/rcmb.2005-0277OC on November 4, 2005
Internet address: www.atsjournals.org

reduced type III to type I collagen ratio (15). Because hyperoxia alone suppresses alveolar epithelial cell proliferation, we assessed the combined effects of BHT plus O_2 on epithelial cell proliferation *in vitro*.

Because caspase-3–mediated apoptosis is increased in ALI (21) and proteolytic cleavage of β-catenin by activated caspase-3 results in disruption of cadherin-mediated homeotypic cell–cell adhesions, and dissociation of E-cadherin from the cytoskeleton and may affect proliferative responses to injury (22), we treated mice with the pan-caspase antagonist z-ASP concomitant with or immediately after BHT/O_2 exposure and assessed the degree of lung injury.

The data presented here are consistent with an association between increased expression of noncanonical β-catenin pathway molecules and the fibroproliferative response to ALI. The data also indicate that apoptosis in early ALI is an important tissue survival mechanism where apoptosis prevents "the worst" (i.e., namely necrosis) or sets the stage for subsequent cell growth (23).

Materials and Methods

Animals and Oxygen Exposures

Male BALB/CJ and C57BL/6 mice (6–8 wk old) were purchased from Jackson Laboratory (Bar Harbor, ME). Mice were maintained in specific pathogen-free conditions and provided with food and water *ad libitum* in accordance with approved institutional policy and protocol. To induce lung injury, mice were treated with a single intraperitoneal injection of 150 or 400 mg/kg 3,5-Di-tert-4butylhydroxytoluene (BHT) (Sigma, St. Louis, MO) in maize oil on Day 0. Control animals were treated with vehicle only. Mice were housed in a large Plexiglas chamber with stable temperature and humidity and strict diurnal light cycling. Food and water were available *ad libitum*. Mice were exposed to a stable 75% O_2 environment for 6 d (condition referred to as BHT/O_2 d6) or room air (21% O_2) as controls. After 6 d, hyperoxia-exposed mice were recovered at 21% O_2 for a further 8 d (BHT/O_2 d6 + d8) or 15 d (BHT/O_2 d6 + d15). Chamber O_2 content was titrated by venturi flow regulator and monitored by continuous oximetry. CO_2 was $< 1\%$ at all times. The survival of BHT/O_2 d6 mice was 100%, versus 92% ± 4% for BHT/O_2 d6 + d15 (P = NS). Survival among vehicle-treated, 75% O_2-exposed mice was 100% at d6, d6 + d8 21% O_2, and d6 + d15 21% O_2, which was consistent with previous reports (24).

In Vivo Caspase Inhibition

To test the effect of caspase inhibition in the development of ALI remodeling triggered by BHT/O_2, mice were treated with the broad-spectrum caspase inhibitor Z-Asp-2,6-dichlorobenzoyloxymethylketone (z-ASP; Alexis, San Diego, CA), 1 mg/mouse (intraperitoneally) dissolved in DMSO ($n = 5$ for each time point). Daily z-ASP treatment was initiated at the time of BHT/O_2 exposure (Day 0).

Tissue Preparation, Histology, and Immunohistochemistry

At various time points, animals were killed by exsanguination under pentobarbital sodium anesthesia (100 mg/kg intraperitoneally). The pulmonary vascular tree was perfused under a fixed distending pressure. The tissues were processed using a number of approaches. Lungs from some mice were inflation fixed at 25 cm H_2O with zinc fixative (Sigma) and later paraffin embedded for histologic analysis. Left lungs from other animals were removed and homogenized in complete protease inhibitor cocktail (Roche Applied Science, Indianapolis, IN) for Western blot analysis, and right lungs were excised for mRNA extraction and analysis. Tissue sections were stained with H&E for histology and evaluated by two independent observers for airspace, septal, and bronchovascular changes, including cellularity, septal distortion, and matrix deposition, compared with 21% O_2 control mice. Immunohistochemistry was performed on deparaffinized tissue sections pretreated with 3% H_2O_2 in methanol for inactivation of endogenous peroxidase. Sections were then placed in 4% normal goat serum for 2 h before incubation with rabbit polyclonal primary antisera against murine β-catenin (1:50; Santa Cruz Biotechnology, Santa Cruz, CA). Sections were incubated with Alexa Fluor 488 goat anti-rabbit IgG (Invitrogen; Molecular Probes, Eugene, OR) and mounted in Vectashield fluorescence mounting medium with 4,6-diamidino-2-phenylindole (DAPI) for nuclear counterstaining (Vector Labs, Burlingame, CA). Negative controls for nonspecific binding included normal rabbit serum without primary antibody or with secondary antibody alone. Sections were evaluated by two-photon microscopy as described below. Separate lung sections were incubated with biotinylated rabbit anti-cyclin D-1 (Santa Cruz Biotechnology). Biotinylation was performed according to the manufacturer's instructions (DakoCytomation, Carpinteria, CA). Sections were counterstained with hematoxylin and examined by light microscopy.

Fluorescent terminal deoxynucleotidyl transferase-mediated dUTP nick end labeling (TUNEL) of DNA strand breaks was performed according to the manufacturer's instructions (Roche Applied Science). Overlapping DAPI in blue and FITC in green create a turquoise, apoptotic-positive signal. Ten randomly selected fields were analyzed for each section. Image analysis was performed with Zeiss image analyzer (KS 300, release 2.0; Carl Zeiss, Thornwood, NY).

Lung Collagen Measurements

For histologic assessment of lung collagens, sections were stained with picro-sirius red (Biocolor, Westbury, NY) and washed with acidified water (0.5% glacial acetic acid) as previously described (25, 26). Mounted sections were examined for birefringence by polarizing light microscopy. For quantitative assessment of total extractable lung collagens, the entire right lungs from three mice per condition were carefully dissected away from mediastinal structures. Each lung was homogenized in 1 ml protein lysis cocktail and Sircol-dye assay (Biocolor) performed as previously published (27) by 96-well colorimetric plate assay (absorbance 540 nm; Perkin Elmer, Boston, MA) and compared with a purified collagen standard.

Western Blot Analysis

Lung protein homogenates (10 μg per animal determined by colorimetric Bradford microplate assay; $n = 5$ per condition) were subjected to 12% SDS-PAGE electrophoretic transfer onto polyvinylidene fluoride membrane (Immobilon-P; Millipore Corp., Bedford, MA) for Western blot analysis The antibodies and supplier used were rabbit anti-murine E-cadherin (1:2,000 dilution) rabbit anti-murine cyclin D-1 (1:500; Santa Cruz Biotech), rabbit anti-murine integrin-linked kinase-1 (ILK-1) (1:1,000 dilution) and rabbit anti-murine cleaved caspase 3 (1:2,000 dilution; Cell Signaling Technology, Inc., Beverly, MA), β-catenin mAb (1:500) and E-cadherin mAb (1:2,000 dilution) (BD Biosciences Pharmingen, San Diego, CA), and β-actin mAb (1:20,000 dilution). After Tween 20 0.1% in TBS washes, the membranes were incubated with relevant horseradish peroxidase–conjugated secondary Ab (Amersham Inc., Arlington Heights, IL) for 1 h. Signal development was performed using an enhanced chemiluminescence detection kit (Amersham). Protein band densitometry was performed with a Gel Doc 2000 running Quantity One 1-D analysis software (Bio-Rad, Hercules, CA).

Cell Culture and *In Vitro* Hyperoxia Exposure

Transformed murine lung epithelial cells (MLE)-12 (American Type Culture Collection, Manassas, VA) were a generous gift from Patty J. Lee (Yale University, New Haven, CT). They were grown to confluence in Dulbecco's modified Eagle's medium containing pH indicator dye (Invitrogen) supplemented with 2% FBS and 10% penicillin-streptomycin (Invitrogen) in a humidified atmosphere in 5% CO_2 and air. Cell monolayers at 70% confluence in tissue-culture treated wells or slides were used in all experiments. Cells were treated with varying concentrations of BHT-QM (28) (generously provided by J. Thompson) or vehicle as control. Hyperoxic exposures were performed by placing cells in sealed modular chambers (Billups-Rothenberg, Del Mar, CA) and flushing the chambers with a gas mixture of 95% O_2-5% CO_2 until equilibrium was detected by in-line oximetry. The chamber entry and exit ports were clamped, and sealed chambers were incubated at 37°C. Chambers were flushed with the 95% O_2-5% CO_2 gas mixture every 24 h if exposures were > 24 h. To evaluate cell viability, MLE-12 cell monolayers were treated with CyQUANT GR dye according to the manufacturer's directions. Plates were analyzed with a fluorescence plate reader (Perkin Elmer, Boston, MA).

RNA Isolation and Analysis

Minced mouse lungs preserved in RNAlater Stabilization Reagent (Qiagen, Valencia, CA) were homogenized and RNA extracted using a Midi Kit (Qiagen). RNA quantification was performed by spectrophotometry, and RNA integrity was confirmed by Agilent bioanalyzer. Equal amounts (1 μg) of RNA were reverse transcribed with a High Capacity cDNA Archive Kit (Applied Biosystems, Foster City, CA). mRNA expression levels for TCF-1,TCF-3, and LEF-1 were evaluated by multiplex RT-PCR (Qiagen) and real-time quantitative PCR. Primer and probe sequences are available on request. Amplified multiplex RT-PCR products were detected using ethidium bromide gel electrophoresis with glyceraldehyde-3-phosphate dehydrogenase (GAPDH) as in internal standard for each sample. Real-time quantitative PCR was performed with specific TaqMan primers and probes using the ABI Prism 7700 Sequence Detector and SDS analysis software (Applied Biosystems). For each transcription factor, the optimal numbers of cycles were determined experimentally. All reactions were performed in triplicate, and a negative control (no RNA template) and positive control (no polymerase) were introduced in each run. Data were analyzed according to the $2^{-\Delta\Delta CT}$ method, and relative mRNA abundance was calculated as percentage of β-actin in each sample.

Two-Photon Imaging and Analysis

A Zeiss LSM 510 NLO two-photon laser scanning confocal microscope maintained by the University of Colorado Health Sciences Center light microscopy facility was used for quantitation of β-catenin nuclear translocation in lung sections from BHT/O_2-treated mice. The system uses a tunable Coherent Mira 70 MHz mode locked Titanium:Sapphire, two-photon infrared laser using a 63X Apochromat oil immersion lens (numerical aperture 1.4, working distance 0.09 mm). Images were generated using a 0.6-μm step size with a scan area at each image plane of 1,024 × 1,024 pixels. Within each section, five arbitrarily chosen areas were selected. Images were converted to TIFF format and processed with LSM 5 Image Browser (Zeiss) and the public domain NIH Image J program (National Institutes of Health, Bethesda, MD) (29).

Statistical Analysis

Normally distributed data are expressed as the mean ± SEM and were assessed for significance by Student's *t* test or ANOVA with post-hoc continuity correction for multiple comparisons as indicated in the text. Non-normally distributed data were assessed for significance using the Wilcoxon rank sum test. Survival parameters were analyzed using the Kaplan-Meier test. Multiple group trends were evaluated with the chi-square test for trends. Statistical calculations were performed using SigmaStat/SigmaPlot software (Systat, Point Richmond, CA). Statistical difference was accepted at $P < 0.05$.

Results

Lung Remodeling after BHT/Hyperoxia-Induced ALI Is Characterized by Epithelial and Interstitial Cell Proliferation and New Collagen Deposition

H&E-stained lung sections from BHT/O_2 d6 mice revealed significant ALI characterized by inflammatory cell infiltrates, epithelial desquamation, and alveolar exudates (Figure 1Ae). Lungs from mice exposed to BHT/O_2 d6 + d8 and BHT/O_2 d6 + d15 showed progressively marked interstitial cellular proliferation, alveolar epithelial cell hyperplasia, foamy alveolar macrophage accumulation, and interstitial matrix deposition (Figures 1Ag and 1Ai). BHT/O_2 d6 + d15 lungs were notable for significant bronchial distortion and areas of subpleural airspace enlargement (Figure 1Ai). By contrast, lungs from normoxia-exposed mice treated with BHT at Day 6 revealed significantly less inflammation; the inflammation resolved after an additional 15 d (Figure 1Ac). Qualitative assessments of lung collagen were made by phase-contrast microscopy of Sirius red–stained lung sections and quantitative colorimetric Sircol assays of whole-lung extractable collagen. There was a marked increase in interstitial birefringent collagen in lungs from BHT/O_2 d6 + d15 (Figure 1Ai) compared with 21% O_2 and BHT/O_2 d6 mice (Figure 1Aa). Compared with 21% O_2 (147.03 ± 7.47 μg/lung), whole-lung collagen was significantly increased in the BHT/O_2 d6 + d8 (197.15 ± 3.35 μg/lung) and BHT/O_2 d6 + d15 groups (190.25 ± 5.16 μg/lung; $P = 0.001$ for both comparisons).

Postinjury Epithelial Proliferation Is Amplified by Combined BHT/Hyperoxia Exposure *In Vitro*

Proliferation of MLE-12 cells exposed to hyperoxia alone for 8 or 24 h was comparable to that for cells incubated in normoxic conditions in the presence or absence of BHT. Cells incubated for 8 h in 95% O_2 followed by 16 or 48 h of normoxic recovery experienced a 1.3- and 1.8-fold relative reduction in proliferation, respectively, compared with 21% O_2 control ($P < 0.01$ for both comparisons) (Figure 2). By contrast, the proliferative rate was preserved after 16 h of normoxic recovery after incubation in the presence of 95% O_2 plus BHT-QM for 8 h (P = NS) but reduced 2.1-fold after 48 h of normoxic recovery compared with 21% O_2 control ($P < 0.01$). However, proliferation after 48 h normoxia was 2.7-fold lower in vehicle-treated compared with BHT-QM–treated cells ($P = 0.027$). These data demonstrate that the proliferation is enhanced during normoxic recovery after combination BHT-QM plus hyperoxia exposure compared with hyperoxia alone.

Postinjury Lung Remodeling Is Associated with Increased E-Cadherin/β-Catenin Expression

Immunoblotting of whole lung lysates from mice at different time points after initial BHT/O_2 exposure demonstrated changes in expression of cadherin-catenin signaling pathway intermediates. In particular, β-actin–normalized E-cadherin expression was reduced 1.59-fold in lysates from BHT/O_2 d6 compared with normoxic vehicle–only controls ($P < 0.01$) (Figure 3A). This was contemporaneous with the period of maximal epithelial injury and morphologic abnormalities. Lung E-cadherin content normalized by Day 15 of normoxic recovery, simultaneous with the peak of cellular proliferation and repair. Associated with the loss of total lung E-cadherin expression was a 1.51-fold increase in total lung expression of β-catenin in BHT/O_2 d6 + d8 lungs relative to 21% O_2 (Figure 3A). This peak occurred after a 20% reduced expression in BHT/O_2 d6 lungs compared with 21% O_2 control. Increased interstitial cell-predominant immunostaining of β-catenin was detected by light microscopic evaluation of immunostained BHT/O_2 d6 + d8 lung sections compared with 21% O_2 control (Figure 3Bv versus 3Bi). Quantitative assessment of processed two-photon colocalization images (five high-power field images per lung; Figure 3C) for a nuclear or cytoplasmic distribution pattern demonstrated significantly increased nuclear colocalization of β-catenin in lung interstitial cells from BHT/O_2 d6 + d15 compared with vehicle/21% O_2 control (chi-square test for trends, $P < 0.0001$) (Figure 4Bviii versus 4Biv).

Enhanced Integrin-Linked Kinase Expression during BHT/Hyperoxia Lung Injury Remodeling

Expression of the cadherin-catenin complex regulator ILK-1 was increased 1.72 ± 0.1-fold in BHT/75% O_2 d6 lungs compared with vehicle/21% O_2 controls ($P < 0.001$) (Figure 3A). ILK-1 levels were further increased 1.85 ± 0.17-fold relative to control in BHT/75% O_2 d6 + d8 and 3.53 ± 0.1 at BHT/75% O_2 d6 + d15 ($P < 0.001$).

β-Catenin Translocation Results in Cotranscriptional Activation and Enhanced Cyclin-D Expression

GAPDH-normalized mRNA expression by multiplex PCR of TCF-1 and LEF-1, but not LEF-3, was increased in BHT/O_2 d6

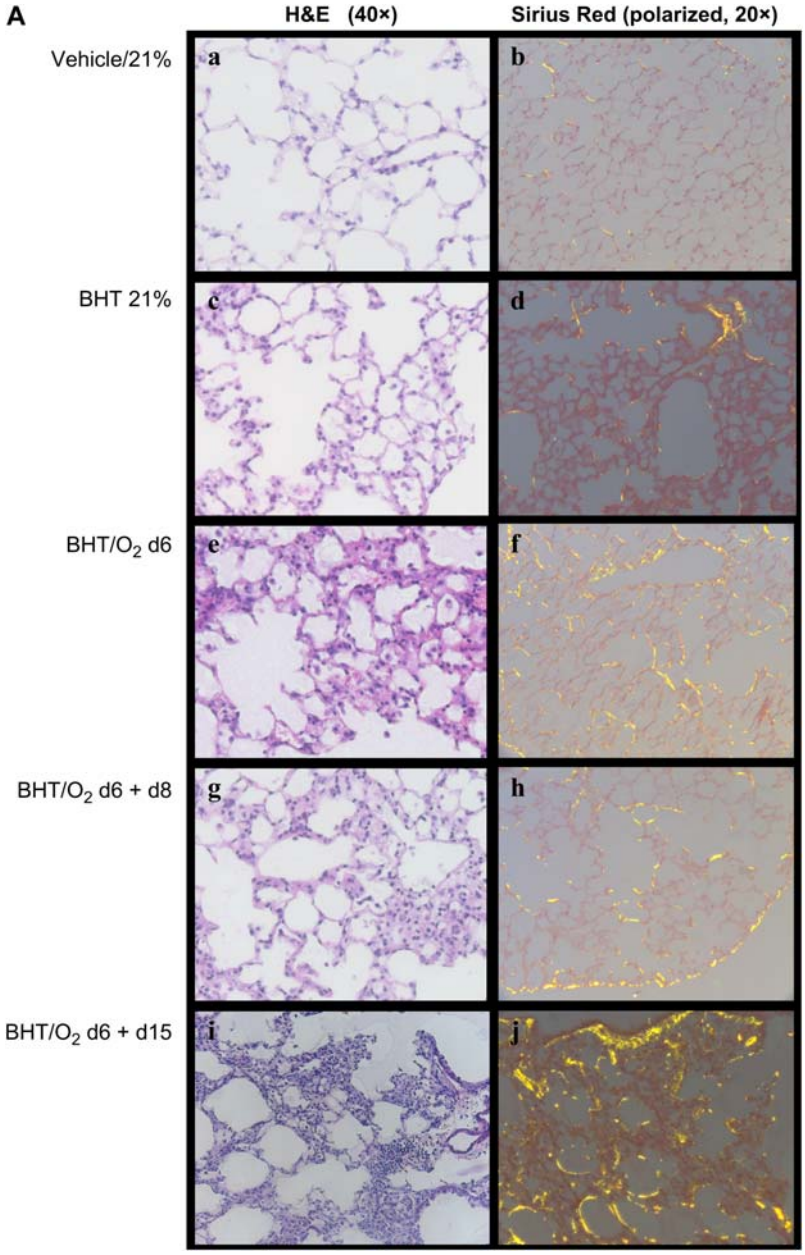

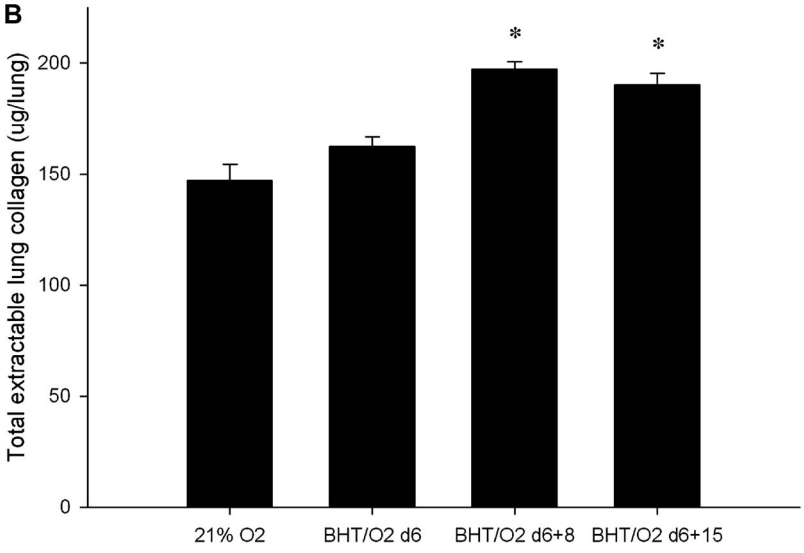

Figure 1. Post BHT/O_2 injury is characterized by monocyte-predominant infiltrates and fibroproliferative changes. (*A*) Representative photomicrographs of zinc-fixed, paraffin-embedded mouse lung sections ($n = 3$ for each condition). H&E (40×, light microscopy) for histopathology (*a*, *c*, *g*, *e*, *i*) and Sirius-red stain (20×, polarizing light microscopy) for immature (green birefringence) and maturing (gold-brown birefringence) collagen (*b*, *d*, *f*, *h*, *j*). (*B*) Total extractable collagen measured by colorimetric Sirius-red assay. Data presented are mean collagen in μg/right lung ± SEM; $n = 3$ right lungs for each condition. *$P = 0.001$ compared with 21% O_2.

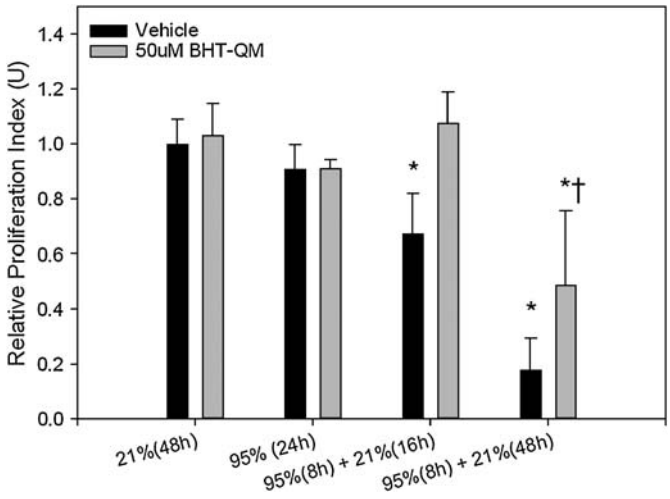

Figure 2. Epithelial proliferation is amplified by combined BHT/hyperoxia exposure compared with hyperoxia alone *in vitro*. Subconfluent MLE-12 cell monolayers seeded in 24-well tissue culture plates were treated with BHT-QM (50 μM) or vehicle and incubated in a sealed normobaric chamber flushed with 95% O_2/5% CO_2 or 21% O_2/5% CO_2 for various time periods and returned to normoxia for up to 48 h. Proliferation by fluorescence assay is expressed relative to vehicle after 48 h at 21% O_2. *$P < 0.01$ compared with 21% (48 h) control. †$P = 0.027$ compared with vehicle at the same time point (95% [8 h] + 21% [48 h]). The data represent mean ± SEM of triplicate wells; $n = 2$ experiments.

and BHT/O_2 d6 + 15 lung, which was consistent with the period of maximal β-catenin expression (Figure 4A). Quantitative GAPDH-normalized TCF-1 expression in BHT/75% O_2 d6 + 15 was 3,276 ± 698.9 copies, compared with 25 ± 22.6 copies in vehicle/21% O_2 controls ($P < 0.05$; ANOVA Neuman Keuls) (Figure 4B).

Expression of the β-catenin transcriptionally regulated cell-cycle protein cyclin D-1 increased 1.91-fold over baseline at BHT/75% O_2 d6 and remained 1.53-fold elevated at BHT/75% O_2 d6 + d15 normoxic recovery (Figure 4C). Cyclin-D1–immunostained lung sections showed a marked increase in areas of alveolar epithelial and interstitial proliferation from BHT/75% O_2 d6, d6 + d8, and d6 + d15 lungs (Figure 4D).

Injury and Remodeling Are Characterized by Enhanced Apoptosis

Actin-normalized expression of whole-lung–activated caspase 3 was increased 3.4-fold in BHT/O_2 d6 lungs and 2.55-fold fold in BHT/O_2 d6 + d15 lungs (Figure 5B) compared with normoxic controls ($P < 0.001$). Immunostained lung sections revealed activated caspase 3 decoration in alveolar interstitium and epithelium and to a lesser extent in bronchial epithelium, most notably in the BHT/O_2 d6 lungs and less prominently in BHT/O_2 D6 + d15 lungs (data not shown). Immunofluorescent TUNEL labeling of lung sections was performed to evaluate the presence of apoptosis and necrosis (Figure 5C). TUNEL-positive cells in the alveolar epithelium and interstitium increased in BHT/O_2 d6 lungs compared with normoxic controls. TUNEL-positive cells were also increased in BHT/O_2 d6 + d15 lungs, particularly in alveolar airspaces.

Caspase Inhibition Amplifies BHT/O_2-Induced Lung Injury

BHT-treated mice injected daily with z-ASP concomitant with 75% O_2 exposure developed substantially amplified and rapidly lethal ALI. No z-ASP treated animals survived the initial 6-d period of hyperoxic exposure (BHT/O_2 + z-ASP median survival was 3 d versus BHT/O_2 vehicle-treated controls; $P < 0.03$) (Figure 5A).Western blotting of whole-lung lysates from z-ASP–treated BHT/O_2 d6 animals confirmed a 39.5 ± 14.1% reduction in actin-normalized cleaved caspase-3 protein expression compared with BHT/d6 vehicle-treated controls ($P = 0.05$, ANOVA, Neuman Keuls) (Figure 5B). Additionally, z-ASP cotreated mice had a reduction in whole-lung β-catenin expression compared with BHT/O_2 d6 controls (Figure 3A). Expression of ILK-1 and E-cadherin was unchanged. Despite standardized immediate postmortem saline flushing of the pulmonary circuit via the right ventricle, histologic evaluation of lungs from mice after 4 and 5 d of treatment ($n = 5$) demonstrated hemorrhagic alveolar airspace filling, vascular microthrombi, diffuse alveolar damage, epithelial desquamation, and substantially increased numbers of alveolar neutrophil and foamy alveolar macrophages (Figure 5Ce). In the face of reduced activated caspase 3 expression, TUNEL-positive cells were equally abundant in BHT/O_2 + z-ASP lungs (Figure 5Cf) as BHT/O_2 vehicle controls.

DISCUSSION

Exuberant fibroproliferative post–lung injury repair results in marked structural abnormalities of the alveolar–capillary interface and long-term impairment of gas exchange. The inflammatory mechanisms underlying the initial phase of ALI have received significant attention, but less is known about the reparative phase. *In vivo* investigations of cellular repair responses to injury have been challenging because lung injury models are fatal or result in an overwhelming fibrotic response (30). Reestablishment of a functional alveolar epithelial–capillary interface requires pulmonary edema resorption, resolution of inflammation, reepithelialization, matrix remodeling, angiogenic recanalization, and endothelial proliferation. This requirement for cellular proliferation, transdifferention, and migration led us to hypothesize that in the injured adult lung, the β-catenin pathway is involved as part of fibroproliferative repair, recapitulating its central role in alveolar bud development during lung organogenesis. To our knowledge, this is the first study to suggest involvement of a noncanonical β-catenin signaling pathway in the proliferative repair phase after sublethal BHT/hyperoxia-mediated murine ALI (summarized in Table 1 and Figure 6). Our findings are consistent with the notion that lung remodeling in response to ALI is regulated in part through cellular pathways that are involved in lung development (9).

To validate the phenotype of postinjury fibroproliferation in this model, we first evaluated histologically the pulmonary effects of BHT/O_2 in mice exposed for 6 d to 75% O_2 and recovered for periods up to 14 d in normoxia. Exposure to hyperoxic environments of 75–85% oxygen content alone induces tolerance to 100% hyperoxia through the induction of antioxidants, including superoxide dismutases (31). Consistent with previous reports (16), the acute effects of BHT/O_2 evaluated at 6 d of hyperoxia involved severe desquamative alveolar damage with intraalveolar hemorrhage, neutrophil infiltration, foamy alveolar exudates, and modest hyaline membranes (Figure 1Ae). Lungs examined from mice after 8 and 15 d of normoxic recovery demonstrated progressive resolution of acute lung injury, alveolar epithelial regeneration, extensive foamy alveolar macrophage, and interstitial lymphocytic infiltrates. This phase was accompanied by interstitial space expansion with fibroblasts, tissue macrophages, and matrix accumulation. Quantitative elevations in lung collagen characterized by Sirius red staining as a progressive accumulation of birefringent perialveolar interstitial

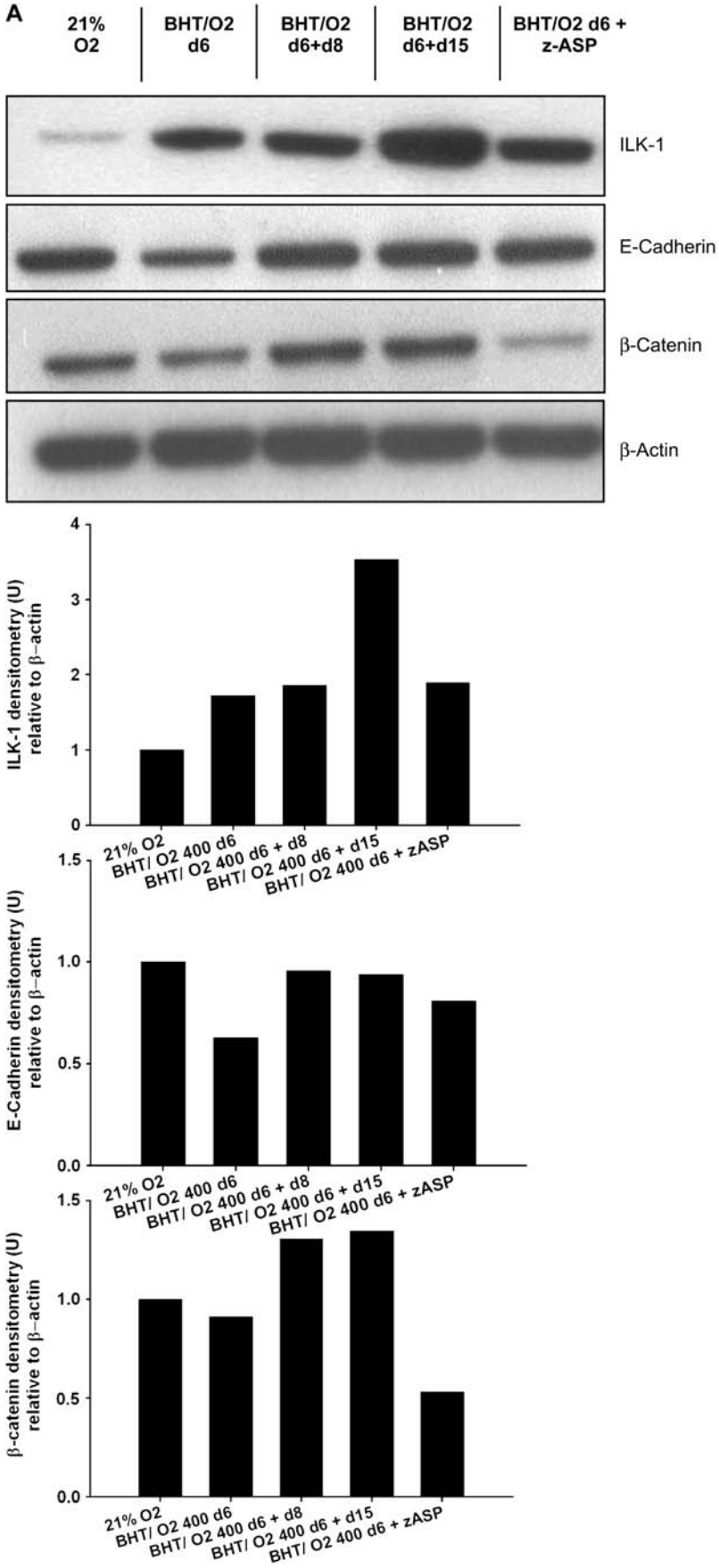

Figure 3. (*A*) Effects of BHT/O_2 injury and repair on cadherin–catenin adherens junction protein expression in whole lung. (*Upper panel*) Representative Western blots of index proteins (first three rows are ILK-1, E-cadherin, and β-catenin, respectively) relative to β-actin (*bottom row*). (*Lower panels*) The graphs represent quantification by densitometry normalized for levels of β-actin. Data are representative of two experiments ($n = 3$ per condition); one of three lungs per condition are shown. (*B*) Nuclear translocation of β-catenin in fibroproliferative ALI repair. Representative photomicrographs of immunohistochemical and immunofluorescence localization of pulmonary β-catenin, zinc fixed, and inflated lung sections from 21% O_2 (*i–iv*) and BHT/O_2 d6 + d15 (*v–viii*) mice demonstrating enhanced interstitial cell-predominant immunostaining (*v*; *arrows*) compared with (*i*) by light microscopy. Two-photon fluorescence microscopy images (representative of three lungs from each group) demonstrate enhanced cytoplasmic and nuclear β-catenin immunofluorescence (red) in overlay (*vi* versus *ii*), monochromatic red channel (*vii* versus *iii*), and two-color colocalization images (*viii* versus *iv*). (*C*) Increased colocalization of nuclear β-catenin in fibroproliferative ALI repair. Two-photon colocalization by two-photon microscopy images were scored for grade and pattern of nuclear pixels as indicated in the inset (1+ minimal perinuclear, 2+ moderate speckled nuclear, 3+ dense nuclear). Autofluorescent alveolar macrophages, identified morphologically, were not included in the quantitative assessment. DAB, diaminobenzidene; Alexafluor 488, pseudocolored red; DAPI, pseudocolored green. The data represent mean ± SEM of five high-power field images per lung; $n = 3$ lungs per condition; chi-square test for trends $P < 0.0001$.

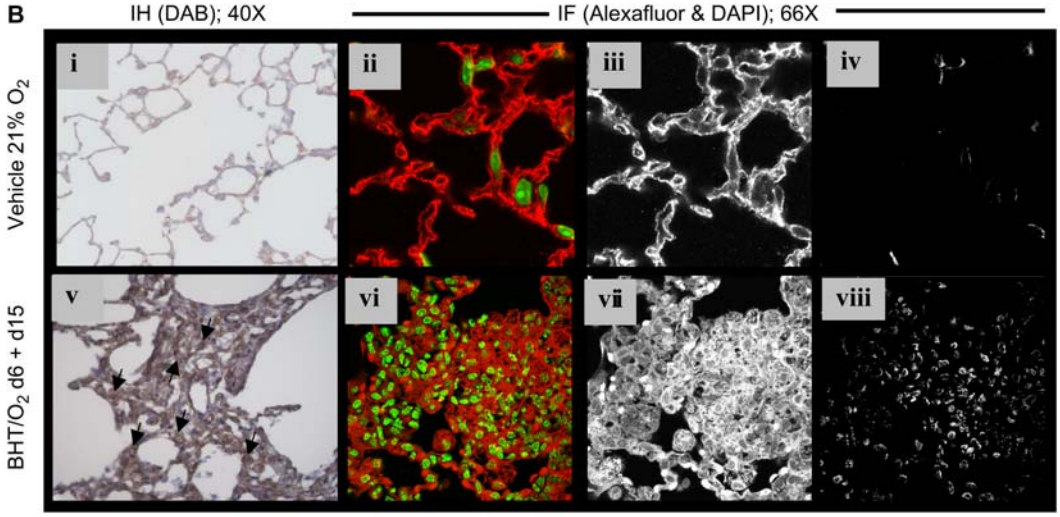

Figure 3. Continued.

collagen were consistent with previous quantitative assessments of increased lung hydroxyproline in this model (15, 16).

To assess whether BHT/O_2 affected epithelial cell survival and proliferation, we examined MLE-12 cell monolayers *in vitro*. This cell line has been used by several investigators to explore the effects of hyperoxia-mediated apoptosis (32, 33). An important difference between the *in vitro* and *in vivo* studies is the use of 95% O_2 in contrast to 75% O_2. This oxygen level was selected for these experiments to address concerns of the relative insolubility of oxygen in the culture medium (34). BHT-QM has been demonstrated to be directly pneumotoxic in BALB/C mouse lungs (35). When compared with hyperoxia or BHT-QM alone, the combination of BHT-QM and hyperoxia followed by 48 h of normoxia resulted in less suppression of proliferation. The mechanism for this potentiation of proliferation may be due in part to the viral transformation of the cell line used in this assay.

Lung interstitial fibroblasts and epithelial cells are the predominant proliferative subpopulations during the normoxic recovery after BHT/O_2 exposure. Epithelial-to-mesenchymal transdifferentiation (EMT) is thought to be an important source for fibroblast generation and proliferation in wound healing and has been suggested as a possible mechanism for the proliferative repair response to BHT/O_2 (36). For this reason, we focused on the noncanonical β-catenin signaling pathway, which is thought to be important in regulating EMT, and its interaction with the adherens junction E-cadherin adhesion protein. β-catenin–dependent EMT may also account for the enhanced matrix turnover and collagen deposition demonstrated in Figure 1.

Total lung E-cadherin was reduced in our study after lung injury and during the early proliferative phase. During the peak of cellular injury and active reparative proliferation, the reduction in E-cadherin would be consistent with a loss of intercellular adherence through tight junctions. Reduced E-cadherin protein expression, in conjunction with nuclear β-catenin localization, has previously been demonstrated in highly proliferative nonneoplastic endometrium (37). Normalization of E-cadherin levels at Day 15 of normoxic recovery post BHT/O_2 suggests a stabilization of the cellular proliferation rate consistent with that previously described in this model (16).

We demonstrated increased whole-lung β-catenin protein levels and nuclear localization in areas of interstitial cellular proliferation contemporaneous with reduced lung E-cadherin expression (Table 1). Although the present studies have not demonstrated increased activity of β-catenin or ILK-1, our findings are consistent with functional activation of the Wnt–β-catenin signaling cascade (38). Additionally, the established regulatory effect of increased ILK-1 expression on E-cadherin transcriptional expression (39) suggests an important role for this serine-threonine kinase in regulating E-cadherin expression in the early postinjury phase when whole-lung ILK-1 expression is increased. ILK-1–mediated E-cadherin repression and inhibition of GSK3β activity (40) has been implicated in EMT (41, 42) and may explain in part the prominent epithelial and interstitial cellular proliferation to BHT/O_2 (15, 16). Bailey and colleagues (43) have shown that peroxide-induced injury of cultured retinal pigment epithelial cells results in reduced junctional N-cadherin protein expression and β-catenin nuclear translocation. This suggests a direct effect of oxidants on epithelial junctional integrity and β-catenin–dependent signaling.

Having demonstrated nuclear accumulation of β-catenin (Figure 3C), we next sought to demonstrate concomitant increases in mRNA expression of the cotranscriptional regulators TCF-1 and LEF-1. In conjunction with increased expression of these molecules, there was an associated increased expression

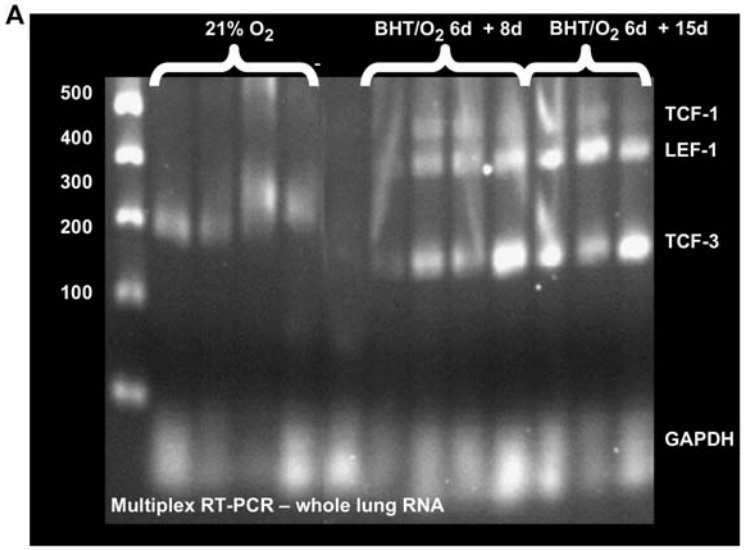

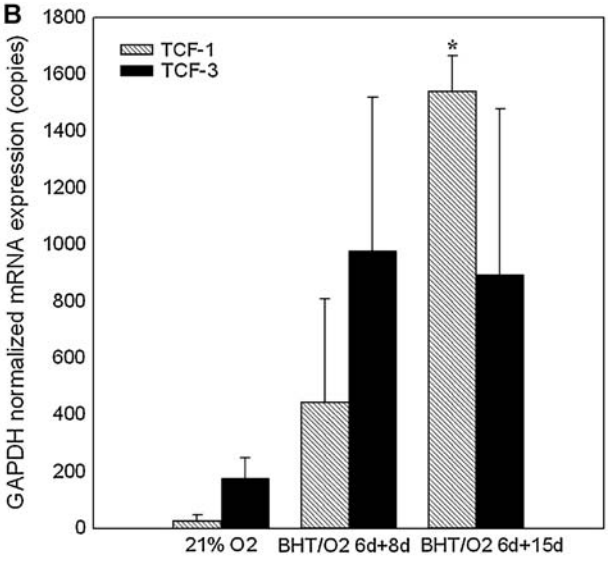

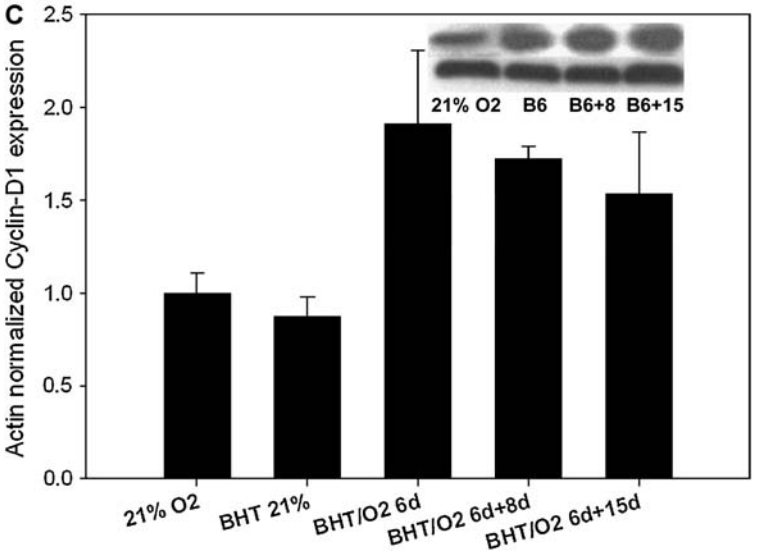

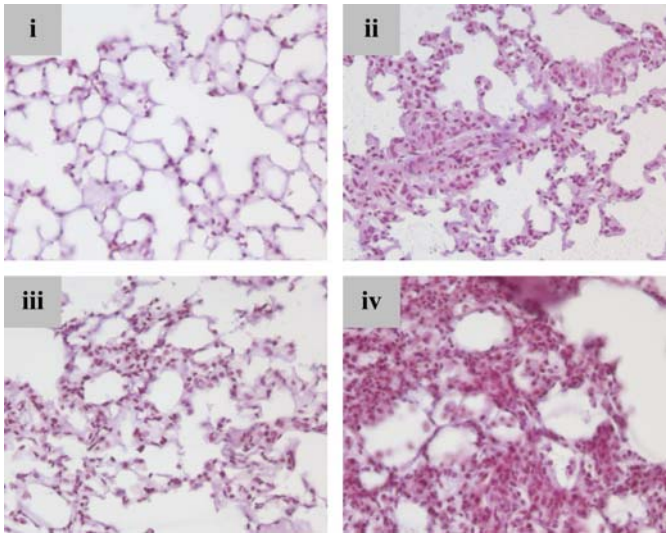

Figure 4. Altered expression of β-catenin cotranscriptional targets in fibroproliferative ALI. (*A*) Expression of TCF-1,3 and LEF-1 by multiplex RTPCR. (*B*) TCF-1 and TCF-3 by real-time qPCR. GAPDH-normalized TCF-1 mRNA copies were increased in whole-lung RNA BHT/O_2 d6 + d15 compared with 21% O_2 control; $n = 3$ or 4 per condition as indicated. *$P < 0.05$. (*C*) Cyclin D1 protein expression is induced in association with increased β-catenin axis expression. Actin-normalized band densitometry of cyclin D1 Western blots from whole lung lysates. The data represent mean ± SEM, $n = 3$ per condition, *$P < 0.05$. Inset is a representative blot (BHT/21% O_2 band not shown). (*D*) Representative photomicrographs of immunohistochemistry for cyclin D1 on lung sections from BHT/O_2–treated mice and controls: (*i*) 21% O_2, (*ii*) BHT/O_2 d6, (*iii*) BHT/O_2 d6 + d8, (*iv*) BHT/O_2 d6 + d15.

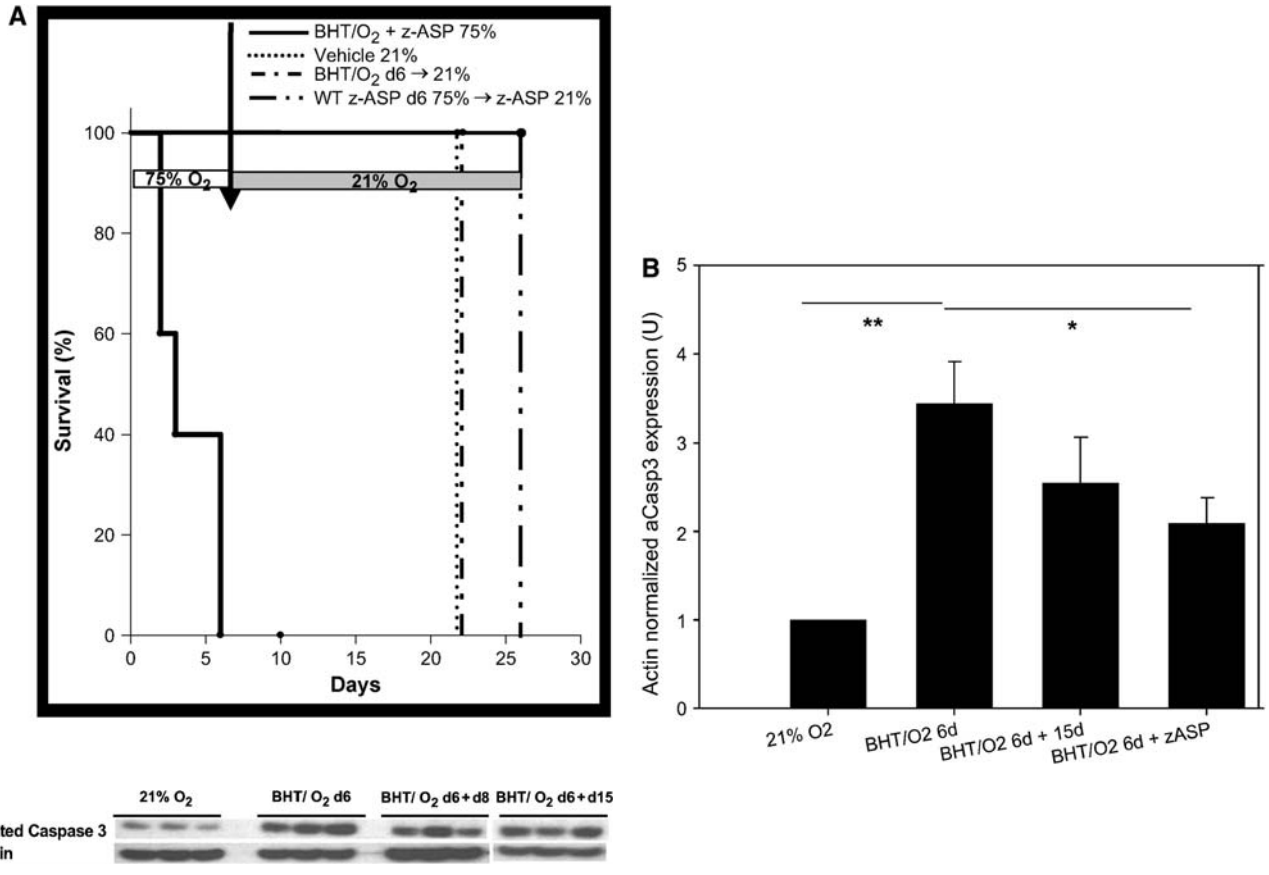

Figure 5. Pharmacologic caspase inhibition amplifies BHT/O_2 ALI by enhanced necrotic cell death. (*A*) Klan-Meier survival curves of BHT/O_2-treated mice. z-ASP cotreatment (100 μg/mouse intraperitoneally daily) during initial BHT/O_2 exposure (BHT/O_2 + z-ASP 75%, *see* Figure 5Ce) amplifies early acute lung injury histologically and results in death by Day 6 compared with DMSO vehicle 21% ($n = 12$) BHT/O_2 d6 → 21% ($n = 12$) and vehicle + z-ASP d6 75% → z-ASP 21% ($n = 5$) (Log rank survival BHT/O_2 + z-ASP 75% versus controls, $P < 0.03$; $n = 10$ per group). (*B*) Densitometric comparison of actin-normalized cleaved caspase-3 expression and representative Western blot of lung lysates from BHT/O_2 d6 + z-ASP compared with BHT/O_2 + vehicle treated animals. The data represent mean ± SEM; $n = 3$ per condition; $^*P < 0.05$; $^{**}P < 0.001$. (*C*) H&E (*a, c, e*) or TUNEL-positive cells (FITC filter) co-stained with DAPI to identify nuclei (*b, d, f*). Numerous TUNEL-positive cells are present in BHT/O_2 d6 (*d*) and z-ASP cotreated lungs (*f*). DAPI, 4′6-diamidine-2-phenylindole-dihydrocholride; TUNEL, terminal deoxynucleotide transferase–mediated dUTP nick end-labeling. Images are representative of 10 high-power fields per lung; $n = 3$ per condition.

TABLE 1. RELATIVE CHANGES IN EXPRESSION OF β-CATENIN PATHWAY INTERMEDIATES DURING BUTYLATED HYDROXYTOLUENE/O_2-INDUCED ACUTE LUNG INJURY AND FIBROPROLIFERATIVE REPAIR

	Phase of BHT/O_2–Induced ALI and Repair			
	21% O_2	BHT/O_2 d6	BHT/O_2 d6 + d8	BHT/O_2 d6 + d15
E-cadherin	++	+	++	++1/2
β-Catenin	+	++	+1/2	++
ILK-1	+	+1/2	++	+++
TCF 1, 3, 4	+	+1/2	++	++
Cyclin D-1	+	+	++	+++
Collagen	+	+	++	++

Definition of abbreviations: ALI, acute lung injury; BHT, butylated hydroxytoluene; ILK, integrin-linked kinase.

Changes are whole-lung protein expression levels (+ to +++) in 21% O_2 mice (except for TCF 1, 3, and 4, which are mRNA levels).

of the LEF-1/β-catenin regulated cell-cycle protein cyclin D1. GSK-3β–mediated inhibition of β-catenin degradation results in cytosolic accumulation, nuclear translocation, and interaction with Tcf/Lef family of transcription factors. These molecules act as downstream cotranscriptional regulators of target genes important in cell-cycle regulation, proliferation, and transdifferentiation. β-catenin/TCF transcriptional complexes have been shown to regulate human cancer cell line proliferation *in vitro* (44, 45).

Increased LEF-1 and TCF-1 mRNA levels could be explained by transcriptional autoinduction mediated by LEF-1 binding domains in the respective promoter sequences of LEF-1 and TCF-1 (46–49). Concomitant LEF-1 and Smad3 HMG box domain binding has been demonstrated to account for cooperative β-catenin and transforming growth factor (TGF) pathway transcriptional control of target gene expression (50). Smad-dependent TGF-β signaling contributes to EMT and is an important profibrotic stimulus (51). The present studies do not preclude an important interaction with TGF-β and other growth factors as part of the proliferative repair response in this model.

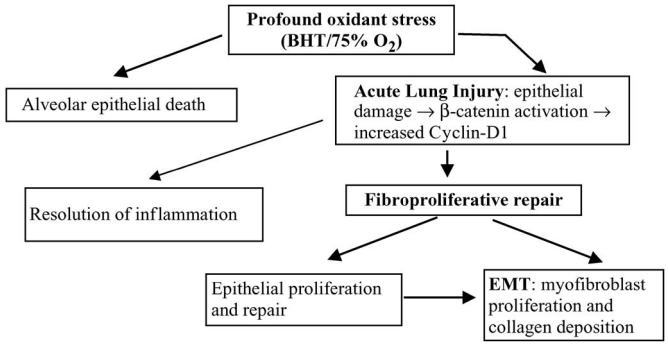

Figure 6. Sequence of BHT/O_2-induced lung injury and β-catenin–mediated repair. Profound oxidant stress (e.g., BHT/O_2) results in alveolar epithelial injury with reduced E-cadherin expression and accumulation of β-catenin. Profound injury can result in cell death. Re-epithelialization and repair is regulated by ILK-1 activation, nuclear β-catenin translocation, enhanced cotranscriptional regulator expression (TCF 1,3), and cyclin D1–mediated cellular proliferation (BHT/O_2 d6 + d8). β-catenin activation also mediates epithelial-to-mesenchymal transition, resulting in transdifferentiation to matrix producing fibroblasts and myofibroblasts. If persistent, this results in lung architectural distortion and fibroproliferation.

Downstream targets of β-catenin/TCF-1/LEF-1 transcriptional regulation include the cell cycle regulatory molecule cyclin D1, which is active in G1 phase transition (52). Through interaction with cyclin-dependent kinase 4, it functions as an important mitogenic regulator. Strong and sustained cyclin D1 induction in proliferative interstitial cells in our model during BHT/O_2 lung injury repair is consistent with enhanced β-catenin/TCF-1/LEF-1–dependent transcriptional activation. However, the contribution of other growth factors, such as epidermal growth factor receptor–mediated stimuli for CycD1 expression, cannot be excluded.

A complimentary mechanism for increased β-catenin expression in this system is through the canonical Wnt-Frizzled receptor pathway (53). The E-cadherin and canonical pathways function through the GSK-3β/Axin/APC complex to regulate β-catenin ubiquitination and proteosomal degradation. The cadherin pathway is thought to regulate the available cytoplasmic β-catenin pool available for Wnt-mediated signaling (54). Activation of the canonical pathway is probable and may play an important role for cellular proliferation disordered lung repair, as previously described in idiopathic pulmonary fibrosis (6).

Lung cellular apoptosis is a dominant mechanism of injury in hyperoxia-mediated ALI (55). Recognition and controlled phagocytic engulfment and removal of apoptotic cells are important in resolution of inflammation. The amplification of acute lung injury in our model with increased early mortality in mice cotreated with the pan-caspase inhibitor z-ASP during BHT/O_2 supports the hypothesis that caspase-mediated apoptosis is a necessary component of lung defenses against overwhelming oxidant stress injury. The presence of TUNEL-positive cells in z-ASP–cotreated lungs is consistent with oxidant-mediated, necrosis-predominant cell death and/or caspase independent apoptosis. z-ASP cotreatment was associated with a relative reduction in β-catenin expression after 6 d of BHT/O_2 exposure, suggesting a caspase-mediated effect on cellular β-catenin turnover. This might be explained by inhibition of caspase-mediated proteolytic cleavage of β-catenin (22) or alternative mechanisms of β-catenin pathway regulation. Although incomplete, the level of caspase 3 inhibition in these studies is comparable to that achieved in studies using chronic z-ASP infusion in rats for periods of up to 1 mo (56). Although the association between increased lung injury and reduced expression of β-catenin in z-ASP–treated, BHT/O_2-exposed mice suggests that caspase-mediated cell death is necessary for β-catenin pathway activation, it is probable that other factors, including secreted Wnt molecules or lysophosphatidic acid, are involved (57).

Because the present findings have been derived from analysis of whole lungs, we recognize that changes of the cadherin-catenin pathway represent aggregate signals from resident lung parenchymal, airway, and migratory inflammatory cells. To address this, we have used immunohistochemical localization to identify the distribution of proteins where possible. However, the contribution of individual cell populations, in particular the contribution of mononuclear leukocytes that are increased in number during the acute inflammatory response, requires future investigation. In addition, the absolute requirement for β-catenin signaling in the fibroproliferative response and the involvement of the canonical Wnt pathway are important questions for future study.

In conclusion, we have demonstrated in a sublethal model of acute lung injury and fibroproliferative remodeling an association with enhanced expression of the cadherin–catenin axis with epithelial regeneration and EMT (Figure 6). We have identified the requirement for caspase-mediated apoptosis as an important survival component of the pulmonary response to acute lung injury.

Conflict of Interest Statement: None of the authors has a financial relationship with a commercial entity that has an interest in the subject of this manuscript.

Acknowledgments: The authors thank John Thompson for reagents, Steven Fadul for assistance with fluorescence microscopy, and John Repine and the Webb Waring Facility staff for animal care and hyperoxia chamber use.

References

1. Adamson IY, Young L, Bowden DH. Relationship of alveolar epithelial injury and repair to the induction of pulmonary fibrosis. *Am J Pathol* 1988;130:377–383.
2. Pan T, Mason RJ, Westcott JY, Shannon JM. Rat alveolar type II cells inhibit lung fibroblast proliferation in vitro. *Am J Respir Cell Mol Biol* 2001;25:353–361.
3. Neff TA, Stocker R, Frey HR, Stein S, Russi EW, Buchser E, Leuenberger P, Chiolero R, Perret C, Freeman J, *et al.* Long-term assessment of lung function in survivors of severe ARDS. *Chest* 2003;123:845–853.
4. Willis BC, Liebler JM, Luby-Phelps K, Nicholson AG, Crandall ED, du Bois RM, Borok Z. Induction of epithelial-mesenchymal transition in alveolar epithelial cells by transforming growth factor-beta1: potential role in idiopathic pulmonary fibrosis. *Am J Pathol* 2005;166:1321–1332.
5. Marshall RP, Bellingan G, Webb S, Puddicombe A, Goldsack N, McAnulty RJ, Laurent GJ. Fibroproliferation occurs early in the acute respiratory distress syndrome and impacts on outcome. *Am J Respir Crit Care Med* 2000;162:1783–1788.
6. Chilosi M, Poletti V, Zamo A, Lestani M, Montagna L, Piccoli P, Pedron S, Bertaso M, Scarpa A, Murer B, *et al.* Aberrant Wnt/beta-catenin pathway activation in idiopathic pulmonary fibrosis. *Am J Pathol* 2003; 162:1495–1502.
7. Shu W, Jiang YQ, Lu MM, Morrisey EE. Wnt7b regulates mesenchymal proliferation and vascular development in the lung. *Development* 2002; 129:4831–4842.
8. Shannon JM, Hyatt BA. Epithelial-mesenchymal interactions in the developing lung. *Annu Rev Physiol* 2004;66:625–645.
9. Mucenski ML, Wert SE, Nation JM, Loudy DE, Huelsken J, Birchmeier W, Morrisey EE, Whitsett JA. Beta-catenin is required for specification of proximal/distal cell fate during lung morphogenesis. *J Biol Chem* 2003;278:40231–40238.
10. Cattelino A, Liebner S, Gallini R, Zanetti A, Balconi G, Corsi A, Bianco P, Wolburg H, Moore R, Oreda B, *et al.* The conditional inactivation of the beta-catenin gene in endothelial cells causes a defective vascular pattern and increased vascular fragility. *J Cell Biol* 2003;162:1111–1122.
11. Reddy R, Buckley S, Doerken M, Barsky L, Weinberg K, Anderson KD, Warburton D, Driscoll B. Isolation of a putative progenitor subpopulation of alveolar epithelial type 2 cells. *Am J Physiol Lung Cell Mol Physiol* 2004;286:L658–L667.
12. Lemercier JN, Meier BW, Gomez JD, Thompson JA. Inhibition of glutathione S-transferase P1–1 in mouse lung epithelial cells by the tumor promoter 2,6-di-tert-butyl-4-methylene-2,5-cyclohexadienone (BHT-quinone methide): protein adducts investigated by electrospray mass spectrometry. *Chem Res Toxicol* 2004;17:1675–1683.
13. Smirnova EG, Lyubimov YI, Malinina TG, Lyubimova EY, Alexandrushkina NI, Vanyushin BF, Kolesova GM, Yaguzhinsky LS. Ionol (BHT) produces superoxide anion. *Biochemistry (Mosc)* 2002;67:1271–1275.
14. Thompson JA, Carlson TJ, Sun Y, Dwyer-Nield LD, Malkinson AM. Studies using structural analogs and inbred strain differences to support a role for quinone methide metabolites of butylated hydroxytoluene (BHT) in mouse lung tumor promotion. *Toxicology* 2001;160:197–205.
15. Haschek WM, Klein-Szanto AJ, Last JA, Reiser KM, Witschi H. Long-term morphologic and biochemical features of experimentally induced lung fibrosis in the mouse. *Lab Invest* 1982;46:438–449.
16. Haschek WM, Reiser KM, Klein-Szanto AJ, Kehrer JP, Smith LH, Last JA, Witschi HP. Potentiation of butylated hydroxytoluene-induced acute lung damage by oxygen: cell kinetics and collagen metabolism. *Am Rev Respir Dis* 1983;127:28–34.
17. Witschi H, Malkinson AM, Thompson JA. Metabolism and pulmonary toxicity of butylated hydroxytoluene (BHT). *Pharmacol Ther* 1989;42: 89–113.
18. Adamson IY, Bowden DH, Cote MG, Witschi H. Lung injury induced by butylated hydroxytoluene: cytodynamic and biochemical studies in mice. *Lab Invest* 1977;36:26–32.
19. Witschi H, Kacew S, Tsang BK, Williamson D. Biochemical parameters of BHT-induced cell growth in mouse lung. *Chem Biol Interact* 1976; 12:29–40.
20. Williamson D, Esterez P, Witschi H. Studies on the pathogenesis of butylated hydroxytoluene-induced lung damage in mice. *Toxicol Appl Pharmacol* 1978;43:577–587.
21. Rudkowski JC, Barreiro E, Harfouche R, Goldberg P, Kishta O, D'Orleans-Juste P, Labonte J, Lesur O, Hussain SN. Roles of iNOS and nNOS in sepsis-induced pulmonary apoptosis. *Am J Physiol Lung Cell Mol Physiol* 2004;286:L793–L800.
22. Brancolini C, Lazarevic D, Rodriguez J, Schneider C. Dismantling cell-cell contacts during apoptosis is coupled to a caspase-dependent proteolytic cleavage of beta-catenin. *J Cell Biol* 1997;139:759–771.
23. Golpon HA, Fadok VA, Taraseviciene-Stewart L, Scerbavicius R, Sauer C, Welte T, Henson PM, Voelkel NF. Life after corpse engulfment: phagocytosis of apoptotic cells leads to VEGF secretion and cell growth. *FASEB J* 2004;18:1716–1718.
24. Jackson RM, Helton ES, Viera L, Ohman T. Survival, lung injury, and lung protein nitration in heterozygous MnSOD knockout mice in hyperoxia. *Exp Lung Res* 1999;25:631–646.
25. Kiernan JA. Sirius red collagen stain. University of Texas Southwestern Medical Center Department of Pathology, 2000. Available from: http://www.histosearch.com/histonet/Oct00A/SiriusredcollagenstainLon.html[cited 2005 May 31]
26. Junqueira LC, Bignolas G, Brentani RR. Picrosirius staining plus polarization microscopy, a specific method for collagen detection in tissue sections. *Histochem J* 1979;11:447–455.
27. Phillips RJ, Burdick MD, Hong K, Lutz MA, Murray LA, Xue YY, Belperio JA, Keane MP, Strieter RM. Circulating fibrocytes traffic to the lungs in response to CXCL12 and mediate fibrosis. *J Clin Invest* 2004;114:438–446.
28. Bolton JL, Sevestre H, Ibe BO, Thompson JA. Formation and reactivity of alternative quinone methides from butylated hydroxytoluene: possible explanation for species-specific pneumotoxicity. *Chem Res Toxicol* 1990;3:65–70.
29. Rasband WS. Image J. U.S. National Institutes of Health, Bethesda, Maryland, 2005. Available from: http://rsb.info.nih.gov/ij/ [cited 2005 May 30]
30. Shen AS, Haslett C, Feldsien DC, Henson PM, Cherniack RM. The intensity of chronic lung inflammation and fibrosis after bleomycin is directly related to the severity of acute injury. *Am Rev Respir Dis* 1988;137:564–571.
31. Crapo JD, Peters-Golden M, Marsh-Salin J, Shelburne JS. Pathologic changes in the lungs of oxygen-adapted rats: a morphometric analysis. *Lab Invest* 1978;39:640–653.
32. Buccellato LJ, Tso M, Akinci OI, Chandel NS, Budinger GR. Reactive oxygen species are required for hyperoxia-induced Bax activation and cell death in alveolar epithelial cells. *J Biol Chem* 2004;279:6753–6760.
33. Romashko J III, Horowitz S, Franek WR, Palaia T, Miller EJ, Lin A, Birrer MJ, Scott W, Mantell LL. MAPK pathways mediate hyperoxia-induced oncotic cell death in lung epithelial cells. *Free Radic Biol Med* 2003;35:978–993.
34. Allen CB, Schneider BK, White CW. Limitations to oxygen diffusion and equilibration in in vitro cell exposure systems in hyperoxia and hypoxia. *Am J Physiol Lung Cell Mol Physiol* 2001;281:L1021–L1027.
35. Kupfer R, Dwyer-Nield LD, Malkinson AM, Thompson JA. Lung toxicity and tumor promotion by hydroxylated derivatives of 2,6-di-tert-butyl-4-methylphenol (BHT) and 2-tert-butyl-4-methyl-6-iso-propylphenol: correlation with quinone methide reactivity. *Chem Res Toxicol* 2002;15:1106–1112.
36. Brody AR, Soler P, Basset F, Haschek WM, Witschi H. Epithelial-mesenchymal associations of cells in human pulmonary fibrosis and in BHT-oxygen-induced fibrosis in mice. *Exp Lung Res* 1981;2:207–220.
37. Shih HC, Shiozawa T, Miyamoto T, Kashima H, Feng YZ, Kurai M, Konishi I. Immunohistochemical expression of E-cadherin and beta-catenin in the normal and malignant human endometrium: an inverse correlation between E-cadherin and nuclear beta-catenin expression. *Anticancer Res* 2004;24:3843–3850.
38. Anderson CB, Neufeld KL, White RL. Subcellular distribution of Wnt pathway proteins in normal and neoplastic colon. *Proc Natl Acad Sci USA* 2002;99:8683–8688.
39. Oloumi A, McPhee T, Dedhar S. Regulation of E-cadherin expression and beta-catenin/Tcf transcriptional activity by the integrin-linked kinase. *Biochem Biophys Acta* 2004;1691:1–15.
40. Tan C, Costello P, Sanghera J, Dominguez D, Baulida J, de Herreros AG, Dedhar S. Inhibition of integrin linked kinase (ILK) suppresses beta-catenin-Lef/Tcf-dependent transcription and expression of the E-cadherin repressor, snail, in APC−/− human colon carcinoma cells. *Oncogene* 2001;20:133–140.

41. Somasiri A, Howarth A, Goswami D, Dedhar S, Roskelley CD. Overexpression of the integrin-linked kinase mesenchymally transforms mammary epithelial cells. *J Cell Sci* 2001;114:1125–1136.
42. de Paulo Castro Teixeira V, Blattner SM, Li M, Anders H-J, Cohen CD, Edenhofer I, Calvaresi N, Merkle M, Rastaldi MP, Kretzler M. Functional consequences of integrin-linked kinase activation in podocyte damage. *Kidney Int* 2005;67:514–523.
43. Bailey TA, Kanuga N, Romero IA, Greenwood J, Luthert PJ, Cheetham ME. Oxidative stress affects the junctional integrity of retinal pigment epithelial cells. *Invest Ophthalmol Vis Sci* 2004;45:675–684.
44. Lin K, Wang S, Julius MA, Kitajewski J, Moos M, Jr, Luyten FP. The cysteine-rich frizzled domain of Frzb-1 is required and sufficient for modulation of Wnt signaling. *Proc Natl Acad Sci USA* 1997;94:11196–11200.
45. Korinek V, Barker N, Morin PJ, van Wichen D, de Weger R, Kinzler KW, Vogelstein B, Clevers H. Constitutive transcriptional activation by a beta-catenin-Tcf complex in APC−/− colon carcinoma. *Science* 1997;275:1784–1787.
46. Filali M, Cheng N, Abbott D, Leontiev V, Engelhardt JF. Wnt-3A/beta-catenin signaling induces transcription from the LEF-1 promoter. *J Biol Chem* 2002;277:33398–33410.
47. Hovanes K, Li TW, Munguia JE, Truong T, Milovanovic T, Lawrence Marsh J, Holcombe RF, Waterman ML. Beta-catenin-sensitive isoforms of lymphoid enhancer factor-1 are selectively expressed in colon cancer. *Nat Genet* 2001;28:53–57.
48. Hovanes K, Li TW, Waterman ML. The human LEF-1 gene contains a promoter preferentially active in lymphocytes and encodes multiple isoforms derived from alternative splicing. *Nucleic Acids Res* 2000;28:1994–2003.
49. Atcha FA, Munguia JE, Li TW, Hovanes K, Waterman ML. A new beta-catenin-dependent activation domain in T cell factor. *J Biol Chem* 2003;278:16169–16175.
50. Labbe E, Letamendia A, Attisano L. Association of Smads with lymphoid enhancer binding factor 1/T cell-specific factor mediates cooperative signaling by the transforming growth factor-beta and wnt pathways. *Proc Natl Acad Sci USA* 2000;97:8358–8363.
51. Cordray P, Satterwhite DJ. TGF-beta induces novel Lef-1 splice variants through a Smad-independent signaling pathway. *Dev Dyn* 2005;232:969–978.
52. Shtutman M, Zhurinsky J, Simcha I, Albanese C, D'Amico M, Pestell R, Ben-Ze'ev A. The cyclin D1 gene is a target of the beta-catenin/LEF-1 pathway. *Proc Natl Acad Sci USA* 1999;96:5522–5527.
53. Nelson WJ, Nusse R. Convergence of Wnt, beta-catenin, and cadherin pathways. *Science* 2004;303:1483–1487.
54. Wheelock MJ, Johnson KR. Cadherin-mediated cellular signaling. *Curr Opin Cell Biol* 2003;15:509–514.
55. He CH, Waxman AB, Lee CG, Link H, Rabach ME, Ma B, Chen Q, Zhu Z, Zhong M, Nakayama K, *et al.* Bcl-2-related protein A1 is an endogenous and cytokine-stimulated mediator of cytoprotection in hyperoxic acute lung injury. *J Clin Invest* 2005;115:1039–1048.
56. Chandrashekhar Y, Sen S, Anway R, Shuros A, Anand I. Long-term caspase inhibition ameliorates apoptosis, reduces myocardial troponin-I cleavage, protects left ventricular function, and attenuates remodeling in rats with myocardial infarction. *J Am Coll Cardiol* 2004;43:295–301.
57. Malbon CC. Beta-catenin, cancer, and G proteins: not just for frizzleds anymore. *Sci STKE* 2005;2005:pe35.